Journal of Power Sources 205 (2012) 439–448

Contents lists available at SciVerse ScienceDirect

Journal of Power Sources

journal homepage: www.elsevier.com/locate/jpowsour

Performance of lithium tetrafluorooxalatophosphate (LiFOP) electrolyte with propylene carbonate (PC)

Liu Zhou, Brett L. Lucht*

Department of Chemistry, University of Rhode Island, 51 Lower College Rd., Kingston, RI 02881, USA

ARTICLE INFO

Article history:
Received 17 December 2011
Received in revised form 5 January 2012
Accepted 6 January 2012
Available online 16 January 2012

Keywords:
Lithium ion batteries
Electrolytes
Propylene carbonate

ABSTRACT

The cycling performance of $LiPF_4(C_2O_4)$ (LiFOP) electrolyte with propylene carbonate (PC) as a cosolvent is compared with $LiPF_6$ electrolyte with ethylene carbonate (EC) as a cosolvent in the presence of different cathode materials, such as $LiNi_{1/3}Co_{1/3}Mn_{1/3}O_2$ and $LiFePO_4$. The cycling performance of cells with LiFOP and PC is similar to cells with $LiPF_6$ with EC at room temperature and superior at low temperature (−10 °C). After thermal abuse the room temperature performance of cells with LiFOP electrolyte and PC is worse than cells with $LiPF_6$ and EC. A detailed analysis of the surface films on both the anode and the cathode via X-ray photoelectron spectroscopy (XPS), scanning electron microscopy (SEM) and Fourier transfer infrared spectroscopy (FT-IR) in the attenuated total reflection (ATR) mode was conducted to provide a better understanding of performance differences.

1. Introduction

Since lithium-ion batteries (LIB) have the highest gravimetric and volumetric energy densities they have become one of the most important commercially produced rechargeable batteries [1]. The incorporation of lithium-ion batteries into portable electronic devices has been occurring for over a decade, but incorporation of LIB into electric vehicles is just beginning. Electric vehicle applications require a superior retention of performance (10–15 years of calendar life) over a greater range of temperatures (−30 to 60 °C). The electrolyte used in commercial lithium-ion batteries are composed of $LiPF_6$ dissolved in organic carbonates or esters, among which ethylene carbonate (EC) is a required component due to the importance of EC in the formation of the anode solid electrolyte interphase (SEI) [2]. However, the required incorporation of EC leads to poor performance at low temperature due to its high melting point (36.4 °C) [3]. Propylene carbonate (PC) is a good candidate for improving low temperature performance due to a low melting point (−48.8 °C), and comparable dielectric constant (65) compared to EC (90) [3]. Unfortunately, replacing EC for PC in a $LiPF_6$ battery, results in continuous electrolyte reduction and exfoliation of the graphite anode [4].

Much effort has been directed toward the development of new salts for the electrolyte of lithium-ion batteries. However, an alternative salt with properties superior to $LiPF_6$ has not been developed. We have been conducting a detailed analysis of a novel salt, lithium tetrafluorooxalatophosphate [$LiPF_4(C_2O_4)$], which shows many comparable properties with $LiPF_6$, including ionic conductivity, electrochemical stability window, and cycling stability [5–9]. However, $LiPF_4(C_2O_4)$ has much better thermal and hydrolytic stability and performance retention upon accelerated aging. While initial investigations of $LiPF_4(C_2O_4)$ with mesocarbon microbead (MCMB) graphite suggested more irreversible capacity during initial formation cycles compared to $LiPF_6$, investigations of natural graphite anodes revealed very similar irreversible capacity during formation cycles for $LiPF_4(C_2O_4)$ and $LiPF_6$ [9]. This unique combination of properties makes $LiPF_4(C_2O_4)$ an interesting alternative to $LiPF_6$. Related investigations of lithium bis(oxalato borate) (LiBOB) uncovered that LiBOB cycled well in PC based electrolytes [10]. The authors concluded that reduction of the LiBOB salt on the anode resulted in the generation of an SEI which prevented graphite exfoliation. It is likely that other oxalate containing salts such as $LiBF_2(C_2O_4)$ and LiFOP would have similar cyclability with PC [11,12]. We report herein an investigation of LiFOP in PC based electrolyte. The cycling properties were investigated with a natural graphite anode and either $LiNi_{1/3}Co_{1/3}Mn_{1/3}O_2$ or $LiFePO_4$ cathodes to confirm reversible cycling behavior of LiFOP/PC electrolytes. A comparison of the low temperature cycling performance of $LiPF_6$/EC electrolyte and $LiPF_4(C_2O_4)$/PC electrolyte was also conducted.

2. Experimental

A standard electrolyte composed of 1.2 M lithium hexafluorophosphate ($LiPF_6$) in 3:7 (vol) ethylene carbonate (EC)/ethylmethyl carbonate (EMC) from Novolyte Corporation

* Corresponding author. Tel.: +1 401 874 5071; fax: +1 401 874 5072.
E-mail address: blucht@chm.uri.edu (B.L. Lucht).

0378-7753/$ – see front matter © 2012 Elsevier B.V. All rights reserved.
doi:10.1016/j.jpowsour.2012.01.067

was used without further purification ($LiPF_6$ electrolyte). Lithium tetrafluorooxalatophosphate, $LiPF_4(C_2O_4)$, was synthesized as described previously [6]. $LiPF_4(C_2O_4)$ (1.2 M) was dissolved in propylene carbonate (PC)/EMC (3:7, vol) to generate the $LiPF_4(C_2O_4)$ electrolyte (LiFOP electrolyte). Battery grade carbonate solvents, PC and EMC, were obtained from Novolyte Corporation.

Coin cells (CR2032) were fabricated in a glove box with argon of high purity. The anodes are natural graphite with carboxymethyl starch (CMS) binder and an active material loading of 6.0 mg cm^{-2}. The cathodes of lithium iron phosphate ($LiFePO_4$) contain $LiFePO_4$ powder with PVDF binder and were obtained from MTI and had an active material loading of 17.5 mg cm^{-2}. The cathode of $LiNi_{1/3}Co_{1/3}Mn_{1/3}O_2$ cells is composed of 92.8% $LiNi_{1/3}Co_{1/3}Mn_{1/3}O_2$ active material, 4.0% PVDF, and 3.2% acetylene black conductive material and was obtained from Lawrence Berkeley National Laboratory (LBNL) and had an active material loading of 13.5 mg cm^{-2}. Between each anode and cathode there is a polypropylene separator which contains 30 μL of electrolyte. The coin cells were cycled with a constant current–constant voltage charge and a constant current discharge between 4.1 V and 3.0 V using a battery cycler (BT-2000 Arbin cycler, College Station, TX). The cells were cycled with the following formation procedures: first cycle at C/20, second and third cycle at C/10 and remaining two cycles at C/5. After the initial five formation cycles the cells were cycled at C/5 rate for 5 cycles at room temperature, then 5 cycles at C/10 rate at −10 °C. A Tenny environmental chamber was used to control the temperature (±1 °C). The cells were sealed with epoxy (Torrseal equivalent, Varian) and stored at 55 °C for one week to simulate accelerated aging. The stored cells were cycled at C/5 rate for 5 cycles at room temperature again, then 5 cycles at C/10 rate at −10 °C. Multiple cells of each type were constructed and cycled with good reproducibility. One set of coin cells were opened for surface analysis after formation cycling, and another set of coin cells were opened for surface analysis after all cycles simulating accelerated aging.

The cells were opened in an Ar glove box after cycling and the electrodes were extracted for surface analysis. The electrodes were rinsed with dimethyl carbonate (DMC) three times prior to surface analysis. The XPS spectra were acquired with a PHI 5500 system using Al Kα radiation ($h\nu$ = 1486.6 eV) under ultra high vacuum. Characterization of XPS peaks was made by recording XPS spectra for reference compounds, which would be present on the electrode surfaces: LiF, Li_2CO_3, $Li_xPO_yF_z$ and lithium alkylcarbonate. The graphite peak at 284.3 eV was used as a reference for the final adjustment of the energy scale in the spectra. Lithium was not monitored due to its low inherent sensitivity and small change of binding energy. The spectra obtained were analyzed by Multipak 6.1A software and fitted using XPS peak software (version 4.1). A mixture of Lorentzian and Gaussian functions was used for the least-squares curves fitting procedure. Scanning electron microscopy (SEM) images were taken on a JEOL 5900 Scanning Electron Microscope. Fourier transfer infrared spectroscopy (FT-IR) was conducted on a Thermo Scientific Nicolet iS10 Spectrometer with an attenuated total reflection (ATR) accessory. The spectra were acquired with a resolution of 4 cm^{-1} and a total of 128 scans.

3. Results and discussion

3.1. Cycling performance

3.1.1. Cycling performance of natural graphite/$LiNi_{1/3}Co_{1/3}Mn_{1/3}O_2$ cells

Lithium-ion coin cells were constructed containing $LiPF_6$ and LiFOP electrolytes and natural graphite/$LiNi_{1/3}Co_{1/3}Mn_{1/3}O_2$ electrodes. The first cycle efficiency of the $LiPF_6$ and LiFOP electrolytes were similar at 87.4% and 88.2%, respectively. After initial formation cycles the cells containing LiFOP electrolyte have a very similar cycling performance to the cells containing $LiPF_6$ electrolyte (Fig. 1). When the cells were cooled to −10 °C for low temperature cycling, the first cycle discharge capacities of both sets of coin cells dropped to ~100 mAh g^{-1}. However, the cells containing LiFOP electrolyte have better discharge capacity retention than the cells containing $LiPF_6$ electrolyte at −10 °C. Then cells were then stored at 55 °C for one week to simulate accelerated aging. After aging, the discharge capacities of both sets of coin cells are reduced compared to the initial room temperature discharge capacities. The discharge capacity of cells containing $LiPF_6$ electrolyte is higher (~130 mAh g^{-1}) than that of cells containing LiFOP electrolyte (~100 mAh g^{-1}). Upon cycling the cells at low temperature (−10 °C) for a second time, both sets of coin cells have poor performance with a low discharge capacity (~35 mAh g^{-1}). The results suggest that while LiFOP can stabilize the anode SEI in the presence of PC at room temperature, upon storage at elevated temperature, 1 week at 55 °C, the protective anode SEI is damaged.

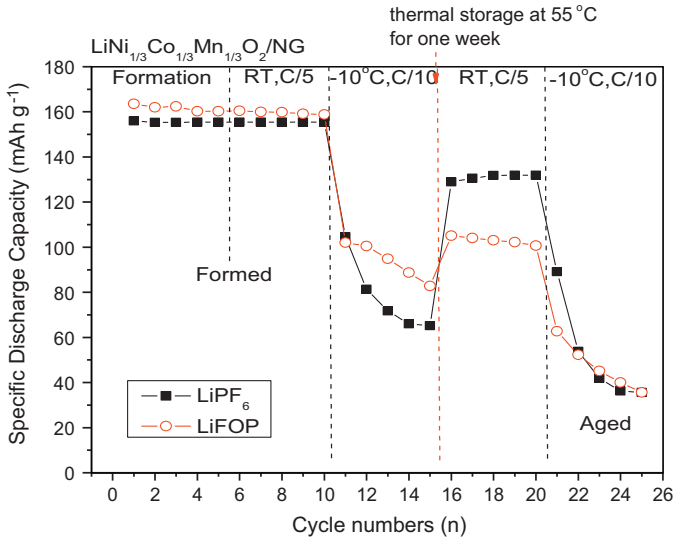

Fig. 1. Cycling performance of 1.2 M $LiPF_6$ in 3:7 EC/EMC and 1.2 M LiFOP in 3:7 PC/EMC in natural graphite/$LiNi_{1/3}Co_{1/3}Mn_{1/3}O_2$ cells.

3.1.2. Cycling performance of natural graphite/$LiFePO_4$ cells

Lithium-ion coin cells (natural graphite/$LiFePO_4$) were constructed with $LiPF_6$ and LiFOP electrolytes. The first cycle efficiency of the $LiPF_6$ and LiFOP electrolytes were similar at 89.9% and 83.9%, respectively. Upon initial formation cycles the cells containing LiFOP electrolyte have slightly higher discharge capacity than the cells containing LiFOP electrolyte (Fig. 2). When the cells were cooled to −10 °C for low temperature cycling, the first cycle discharge capacities of both sets of coin cells dropped significantly. However, the cells containing LiFOP electrolyte retained more capacity (49 mAh g^{-1}) than the cells containing $LiPF_6$ electrolyte (12 mAh g^{-1}). After low temperature cycling the cells were stored at 55 °C for one week and then cycled at room temperature. The discharge capacity of the aged cells containing $LiPF_6$ electrolyte is higher (~110 mAh g^{-1}) than that of aged cells containing LiFOP electrolyte (~80 mAh g^{-1}). The cells were returned to −10 °C. Both sets of cells have very poor low temperature performance after accelerated aging (≤10 mAh g^{-1}). These results are quite similar to what was observed from natural graphite/$LiNi_{1/3}Co_{1/3}Mn_{1/3}O_2$ electrodes.

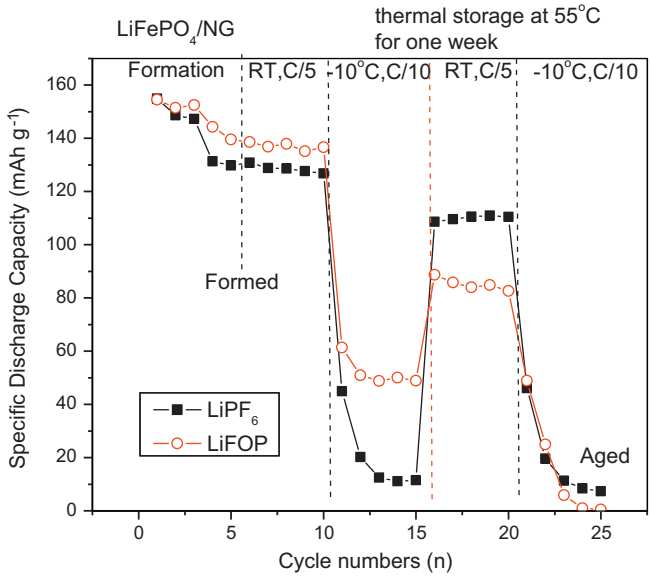

Fig. 2. Cycling performance of 1.2 M $LiPF_6$ in 3:7 EC/EMC and 1.2 M LiFOP in 3:7 PC/EMC in natural graphite/$LiFePO_4$ cells.

3.2. SEM analysis

The SEM images of a natural graphite anode fresh and cycled with a $LiNi_{1/3}Co_{1/3}Mn_{1/3}O_2$ cathode are provided in Fig. 3. After formation cycles, only small changes have occurred to the surface of the anodes in both electrolytes (Fig. 3b and c). The surface of the anode materials after formation with either electrolyte contains a thin amorphous coating consistent with the formation of an SEI. The surface coverage is similar for both electrolytes. The aged $LiPF_6$ anode is very similar to the formed $LiPF_6$ anode, however, the surface of the aged LiFOP anode is different than the formed LiFOP anode (Fig. 3d and e). The particles of the aged LiFOP appear severely damaged or covered by a thick SEI layer.

The SEM images of the $LiNi_{1/3}Co_{1/3}Mn_{1/3}O_2$ cathode fresh and cycled with a natural graphite anode are provided in Fig. 4. There are no apparent changes either after formation or aging. The surface morphology is retained.

The SEM images of a natural graphite anode fresh and cycled with a $LiFePO_4$ are provided in Fig. 5. After formation, there are only small changes occurring to the surface of the anodes cycled with different electrolytes (Fig. 4b and c). The surface of the anode materials after formation with either electrolyte contains a thin amorphous coating consistent with the formation of an SEI. After accelerated aging a significant difference is observed between the anodes. On the surface of anode aged with $LiPF_6$ electrolyte, a thicker surface coating is observed compared to the anode after formation cycling with $LiPF_6$ electrolyte, but the original natural graphite particles are retained (Fig. 4d). The anode aged with LiFOP (Fig. 4e) electrolyte appears very different than the anode after formation cycling with LiFOP electrolyte. The anode surface is a uniform layer of small particles. The original structure of the natural graphite particles is no longer observed. This suggests accelerated aging of the LiFOP electrolyte significantly damages the anode surface or a thick layer of SEI is generated on the anode surface. The changes to the anode structure are similar to the observation of anode samples from natural graphite/$LiNi_{1/3}Co_{1/3}Mn_{1/3}O_2$ coin cells, as discussed above.

The SEM images of a $LiFePO_4$ cathode fresh and after cycling with $LiPF_6$ and LiFOP electrolytes are provided in Fig. 6. The surface of either formed or aged cathodes of both electrolytes look very similar to the fresh cathode, suggesting that any changes occurring to the surface are small.

3.3. XPS analysis

The XPS element spectra of natural graphite anodes fresh and after cycling with a $LiNi_{1/3}Co_{1/3}Mn_{1/3}O_2$ cathode are provided in Fig. 7 and the elemental concentrations are summarized in Table 1. The fresh anode is primarily composed of C (85.0%) with a low concentration of O (15.0%) due to the CMS binder. The C1s spectrum is dominated by the peak characteristic of graphite at 284.3 eV. The peak at 532.5 eV in O1s spectrum is the characteristic peak of the CMS binder. There are no peaks observed in the F1s or P2p spectra.

The surface of the anode after formation cycling with $LiPF_6$ electrolyte is altered and consistent with the formation of an anode SEI.

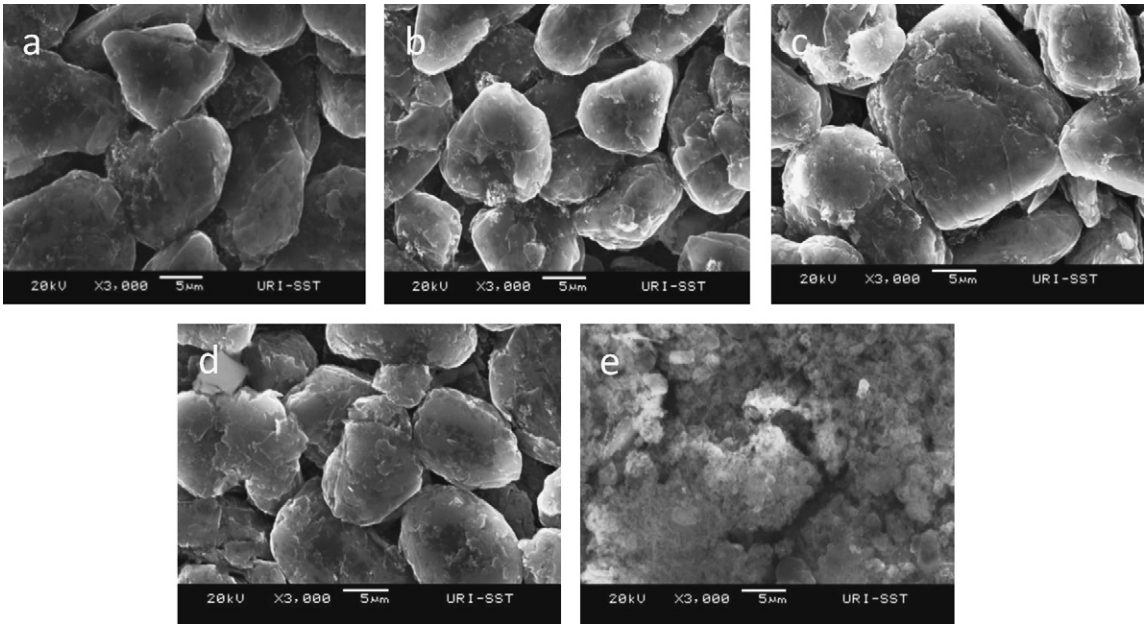

Fig. 3. SEM images of natural graphite anode cycled with $LiNi_{1/3}Co_{1/3}Mn_{1/3}O_2$ cathode (a) fresh; (b) formed with 1.2 M $LiPF_6$ in 3:7 EC/EMC; (c) formed with 1.2 M LiFOP in 3:7 PC/EMC; (d) aged with 1.2 M $LiPF_6$ in 3:7 EC/EMC; (e) aged with 1.2 M LiFOP in 3:7 PC/EMC.

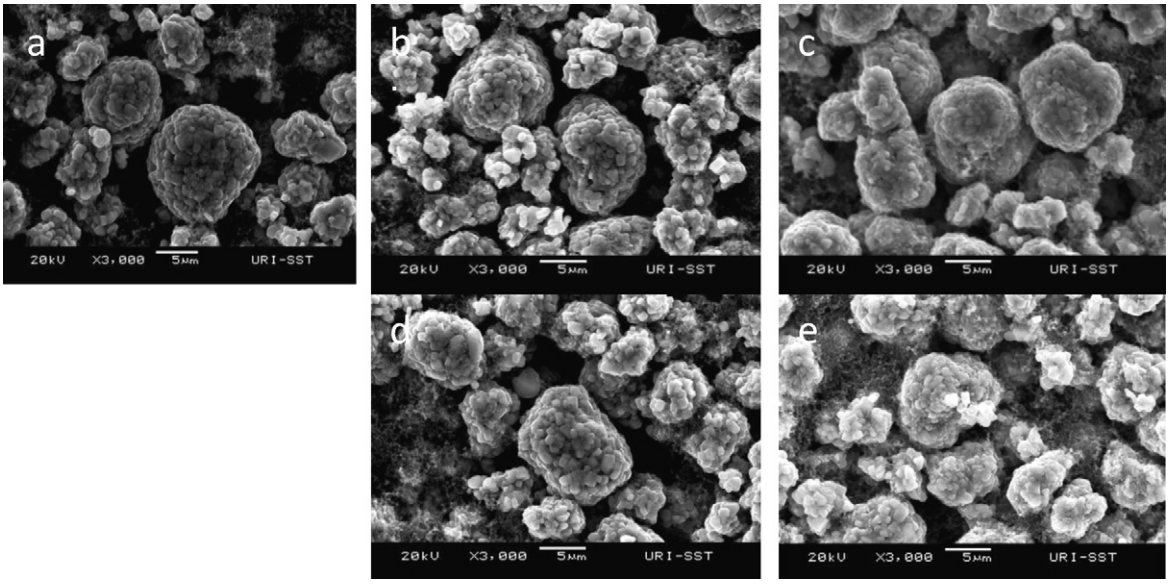

Fig. 4. SEM images of $LiNi_{1/3}Co_{1/3}Mn_{1/3}O_2$ cathode (a) fresh; (b) formed with 1.2 M $LiPF_6$ in 3:7 EC/EMC; (c) formed with 1.2 M LiFOP in 3:7 PC/EMC; (d) aged with 1.2 M $LiPF_6$ in 3:7 EC/EMC; (e) aged with 1.2 M LiFOP in 3:7 PC/EMC.

Table 1
Elemental analysis of natural graphite anode cycled with $LiNi_{1/3}Co_{1/3}Mn_{1/3}O_2$ cathode.

	C1s (%)	O1s (%)	F1s (%)	P2p (%)
Fresh NG	85.0	15.0		
Formed $LiPF_6$	68.9	21.6	9.5	
Aged $LiPF_6$	45.3	42.3	10.5	1.9
Formed LiFOP	48.2	31.5	15.4	4.9
Aged LiFOP	29.9	41.7	22.8	5.6

The concentration of carbon is decreased, while the concentrations of O and F are increased. Peaks characteristic of lithium alkylcarbonates are present in C1s spectrum at ~289.5 eV and 286.5 eV and in the O1s spectrum at 531.6 eV and 533.5 eV. In the F1s spectrum, a peak characteristic of LiF is observed at 685.0 eV. The anode extracted from a cell containing $LiPF_6$ electrolyte after accelerated aging has some differences compared to the anode after formation cycling. The peaks characteristic of lithium alkylcarbonates have greater intensity in both the C1s and O1s spectra. There is an additional peak characteristic of $Li_xPO_yF_z$ at 687.0 eV in F1s spectrum and at ~135 eV in P2p spectrum.

The surface chemistry of the anode after formation cycling with LiFOP electrolyte is different from the anode containing $LiPF_6$ electrolyte after formation cycling. The concentration of carbon is lower (48.2%) than observed for the anode cycled with $LiPF_6$ electrolyte after formation cycling (68.9%), and the concentration of O and F are higher suggesting a thicker anode SEI. Analysis of C1s spectrum reveals that in addition to the peak for graphite at 284.3 eV and peak for C—H containing species at 285.0 eV, the peaks characteristic of lithium alkyl carbonates and polycarbonates are observed at ~289.5 eV (C═O) and ~286.5 eV (C—O). There is also a peak characteristic of oxalate containing species at 288 eV. The related O1s

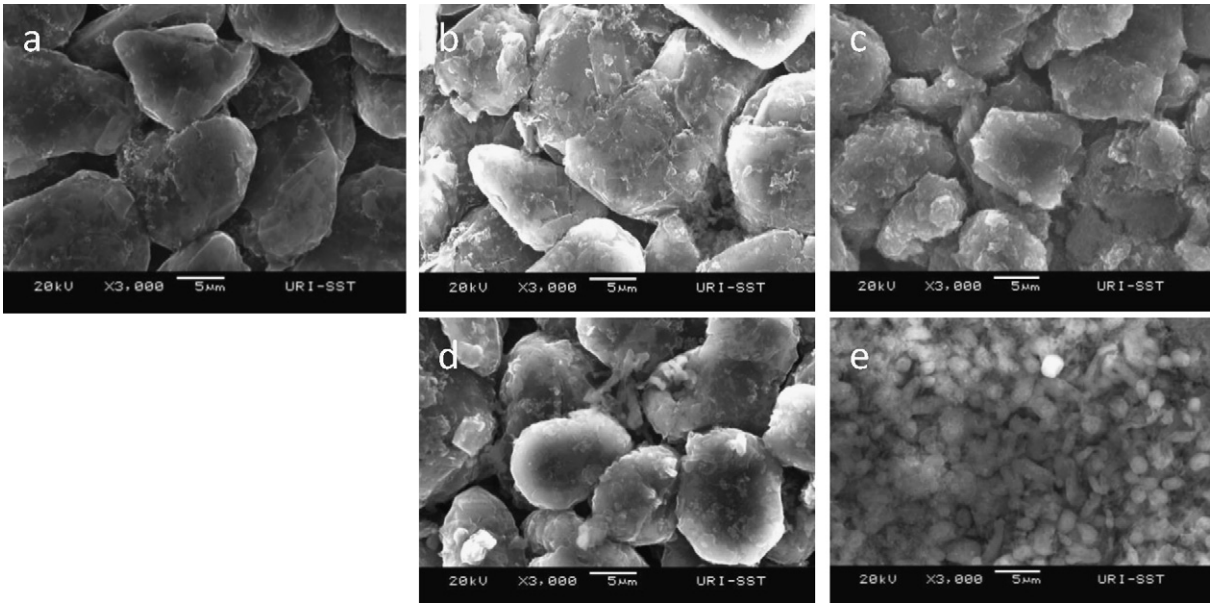

Fig. 5. SEM images of natural graphite anode cycled with $LiFePO_4$ cathode (a) fresh; (b) formed 1.2 M $LiPF_6$ in 3:7 EC/EMC; (c) formed with 1.2 M LiFOP in 3:7 PC/EMC; (d) aged 1.2 M $LiPF_6$ in 3:7 EC/EMC; (e) aged with 1.2 M LiFOP in 3:7 PC/EMC.

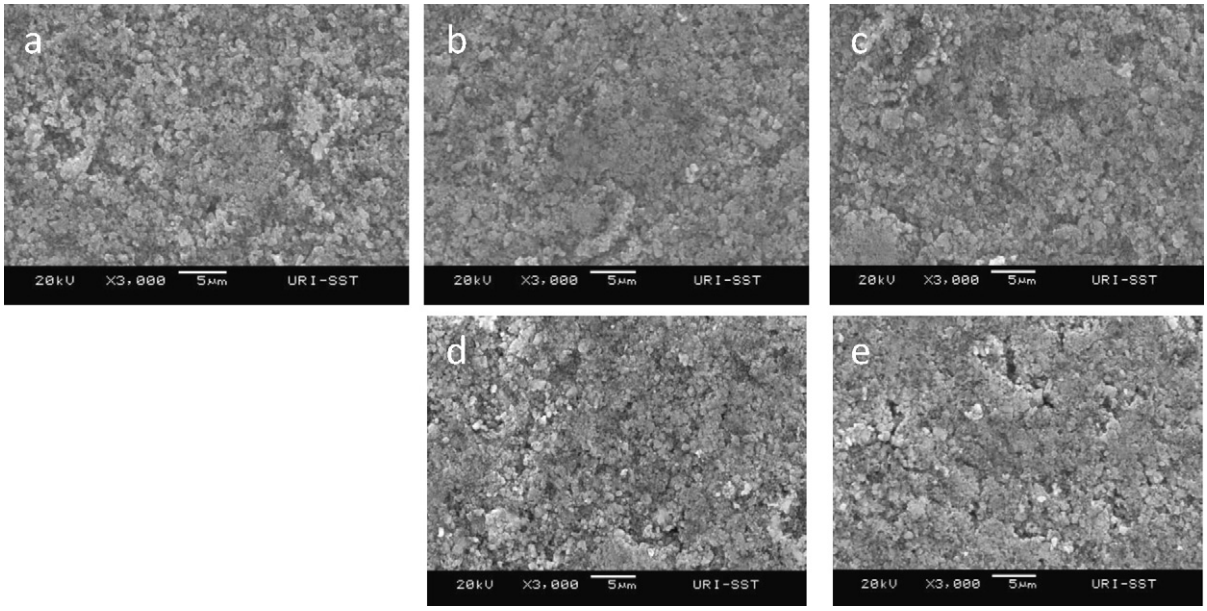

Fig. 6. SEM images of $LiFePO_4$ cathode (a) fresh; (b) formed with 1.2 M $LiPF_6$ in 3:7 EC/EMC; (c) formed with 1.2 M LiFOP in 3:7 PC/EMC; (d) aged with 1.2 M $LiPF_6$ in 3:7 EC/EMC; (e) aged with 1.2 M LiFOP in 3:7 PC/EMC.

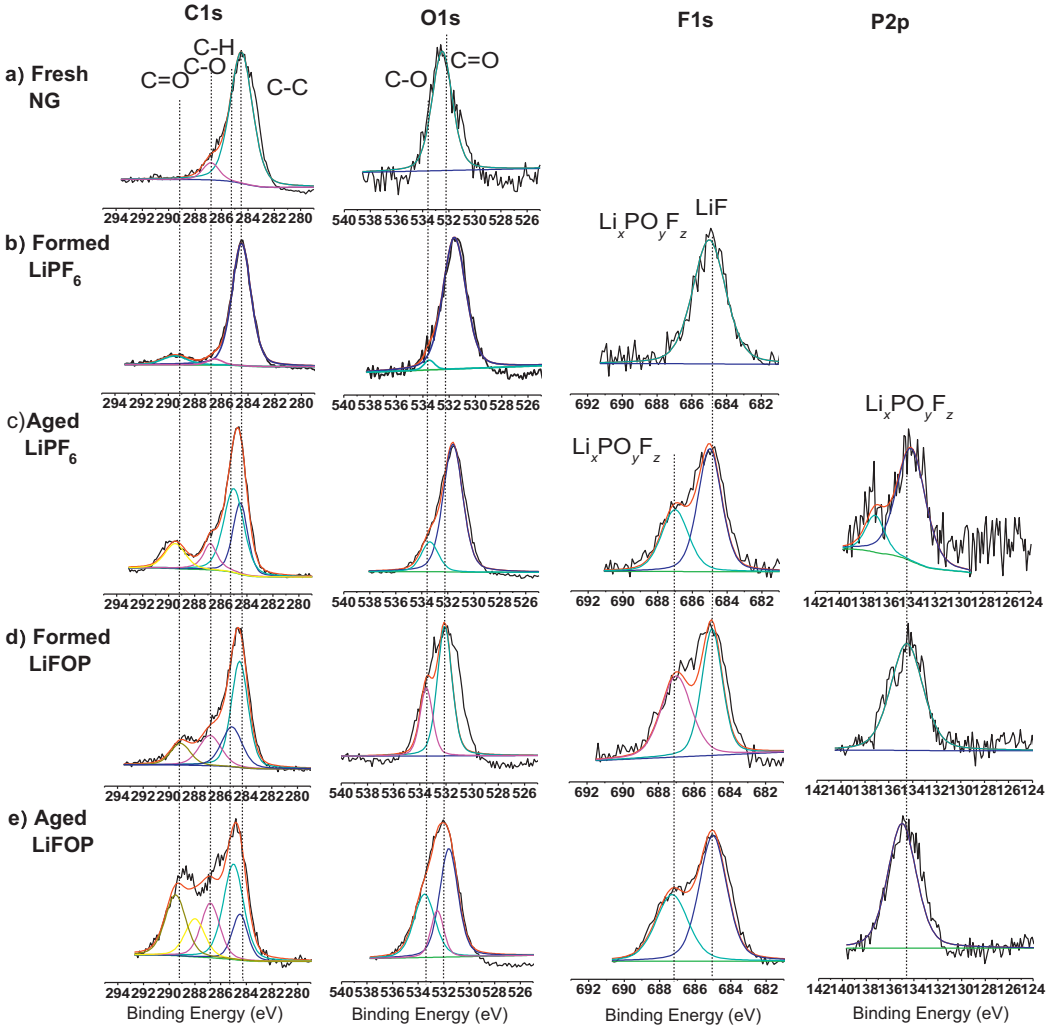

Fig. 7. XPS spectra of natural graphite anode cycled with $LiNi_{1/3}Co_{1/3}Mn_{1/3}O_2$ cathode (a) fresh; (b) formed with 1.2 M $LiPF_6$ in 3:7 EC/EMC; (c) formed with 1.2 M LiFOP in 3:7 PC/EMC; (d) aged with 1.2 M $LiPF_6$ in 3:7 EC/EMC; (e) aged with 1.2 M LiFOP in 3:7 PC/EMC.

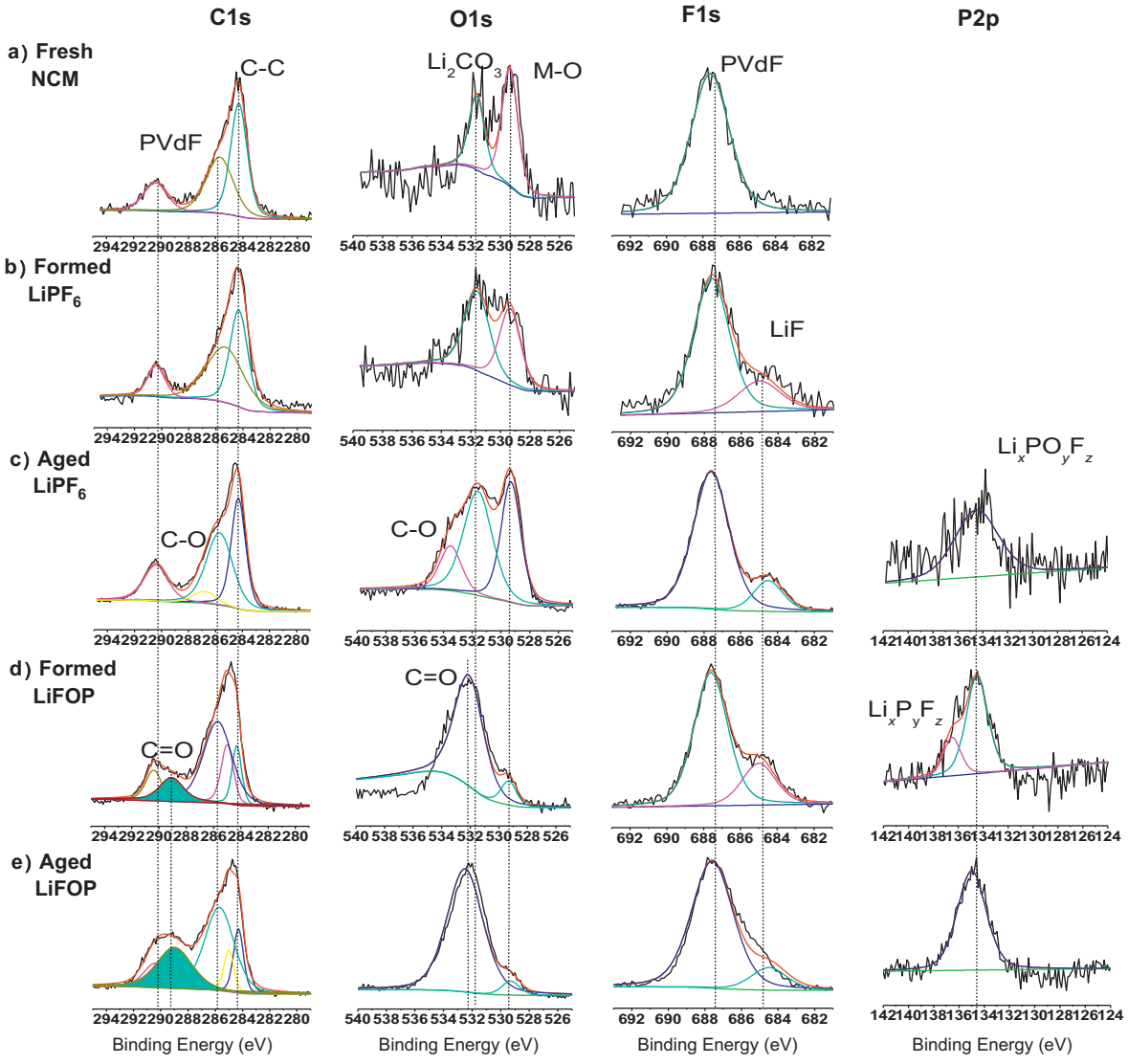

Fig. 8. XPS spectra of $LiNi_{1/3}Co_{1/3}Mn_{1/3}O_2$ cathode (a) fresh; (b) formed with 1.2 M $LiPF_6$ in 3:7 EC/EMC; (c) formed with 1.2 M LiFOP in 3:7 PC/EMC; (d) aged with 1.2 M $LiPF_6$ in 3:7 EC/EMC; (e) aged with 1.2 M LiFOP in 3:7 PC/EMC.

peaks characteristic of C—O (533.5 eV) and C=O (531.6 eV) are also present. Differences are also detected in the F1s spectra. An additional peak characteristic of $Li_xPO_yF_z$ is observed at 687.0 eV. The corresponding P2p peak for $Li_xPO_yF_z$ is also observed at ~135 eV. After aging the concentration of C is lowered and the concentrations of O, F, and P are increased consistent with a thicker anode SEI. The spectra of the aged LiFOP anode are similar to that of the formed anode except that the intensity of the peak characteristic of oxalates at 288 eV in C1s spectrum has greater intensity.

The XPS element spectra of $LiNi_{1/3}Co_{1/3}Mn_{1/3}O_2$ cathodes fresh and cycled with natural graphite electrodes are provided in Fig. 8 and the elemental concentrations are summarized in Table 2. Surface analysis of the cathode after formation cycling with $LiPF_6$ electrolyte indicates that the concentration of C is decreased, while the concentration of O and F are increased. The C1s spectrum of fresh $LiNi_{1/3}Co_{1/3}Mn_{1/3}O_2$ contains three peaks, a peak for graphite at 284.3 eV and peaks for PVdF at 285.7 eV and 290.4 eV. The peak characteristic of PVdF can also be seen in F1s spectrum at 687.6 eV. The O1s spectrum contains a peak at 529.4 eV characteristic of metal oxide (M—O) bond, and the peak at 531.6 eV from residual Li_2CO_3 on the cathode surface. After formation cycling with $LiPF_6$ electrolyte, a new peak is observed in the F1s spectrum at 685.0 eV, which supports the formation of lithium fluoride on the surface of the cathode. The C1s and O1s spectra are very similar to the fresh cathode although the concentrations of C and O are slightly lower. The elemental concentration of the aged $LiNi_{1/3}Co_{1/3}Mn_{1/3}O_2$ cathode in $LiPF_6$ electrolyte is similar with that of the formed $LiNi_{1/3}Co_{1/3}Mn_{1/3}O_2$ cathode except that there is a low concentration of P present on the surface of the aged electrode consistent with the deposition of electrolyte decomposition products. The C1s, O1s and F1s element spectra are also very similar to the fresh cathode. However, a P2p peak characteristic of $Li_xPO_yF_z$ can be detected at 134.5 eV. The results suggest that there are only small changes occurring to the cathode surface upon both formation cycling and accelerated aging with $LiPF_6$ electrolyte.

Table 2
Elemental analysis of $LiNi_{1/3}Co_{1/3}Mn_{1/3}O_2$ cathode.

	C1s (%)	O1s (%)	F1s (%)	P2p (%)
Fresh NCM	65.3	13.2	21.5	
Formed $LiPF_6$	59.6	16.6	23.8	
Aged $LiPF_6$	53.9	17.8	27.6	0.7
Formed LiFOP	45.0	25.5	25.3	4.2
Aged LiFOP	38.5	33.1	24.9	3.5

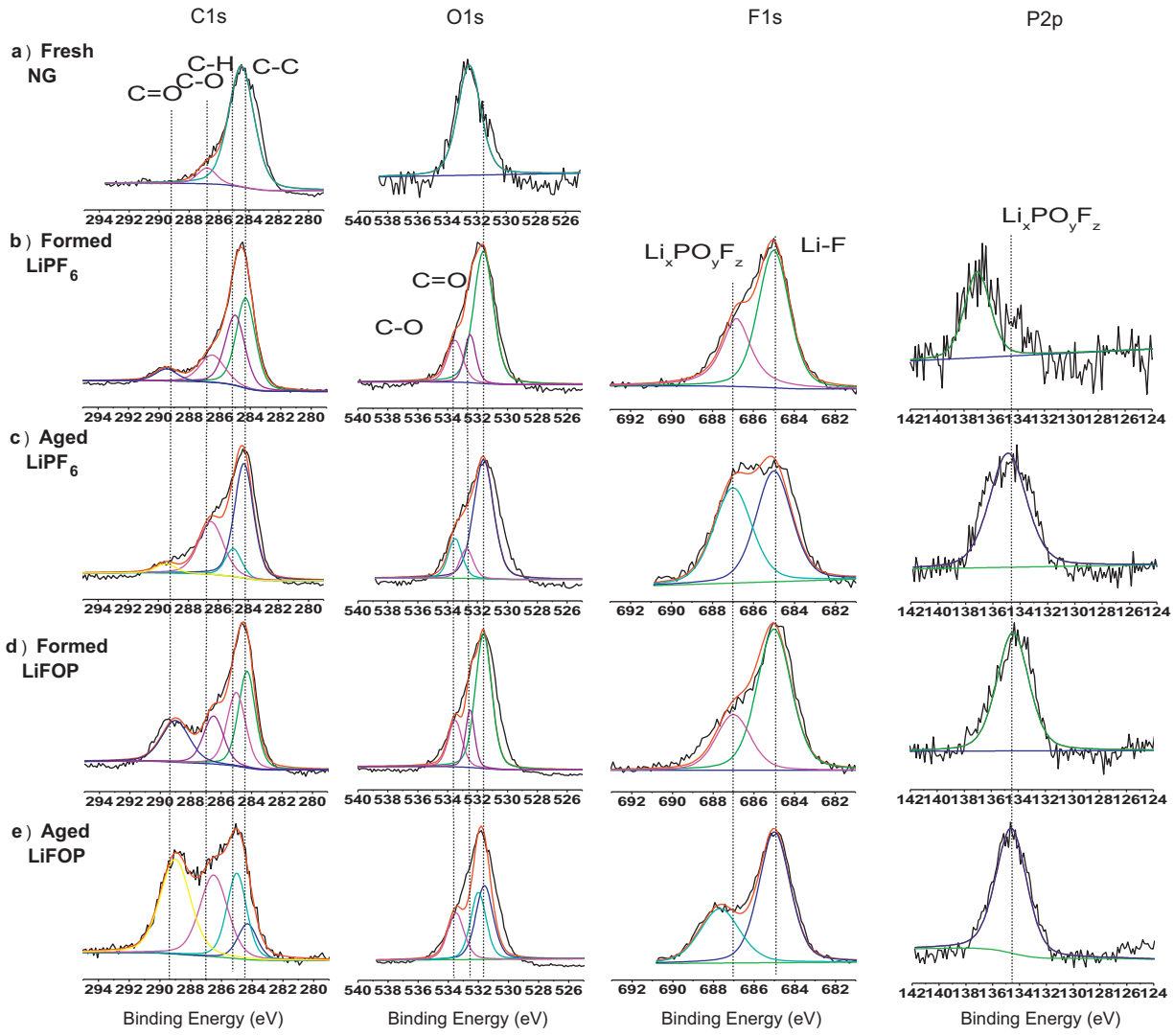

Fig. 9. XPS spectra of natural graphite anode cycled with $LiFePO_4$ cathode (a) fresh; (b) formed with 1.2 M LiFOP in 3:7 EC/EMC; (c) formed with 1.2 M LiFOP in 3:7 PC/EMC; (d) aged with 1.2 M LiFOP in 3:7 EC/EMC; (e) aged with 1.2 M LiFOP in 3:7 PC/EMC.

Significant changes in the concentrations of C and O are observed on the surface of the $LiNi_{1/3}Co_{1/3}Mn_{1/3}O_2$ cathodes after formation cycling or accelerated aging with LiFOP electrolyte. The concentration of C is decreased significantly while the concentration of O and P are increased significantly and the concentration of F is slightly increased. The changes are consistent with the generation of a cathode surface film composed of electrolyte decomposition products. The aged $LiNi_{1/3}Co_{1/3}Mn_{1/3}O_2$ cathode cycled with LiFOP electrolyte has an even lower concentration of C and higher concentration of O, suggesting that the film formed on the aged sample is thicker than the film on the formed sample. The element spectra of the $LiNi_{1/3}Co_{1/3}Mn_{1/3}O_2$ cathode after formation cycling and after accelerated aging with LiFOP electrolyte are very similar. The O1s peak characteristic of M—O becomes smaller, indicating a thick coating on the surface of the cathode. The peaks characteristic of C—O and C═O containing species including lithium alkyl carbonates and oxalates are observed at 286.5 eV and 289.5 eV in C1s spectrum and 533.5 eV and 531.5 eV in O1s spectrum, respectively.

The XPS element spectra of natural graphite anodes fresh and cycled with $LiFePO_4$ cathodes are provided in Fig. 9 and the elemental concentrations are summarized in Table 3. The trend in change of elemental concentrations observed in Table 3 is similar to the trend in Table 1 suggesting similar surface chemistry. After formation cycling with $LiPF_6$ electrolyte, peaks characteristic of C—O and C═O containing species are observed in C1s spectrum and O1s spectrum and peaks characteristic of LiF and $Li_xPF_yO_z$ are observed in the F1s and P2p spectra. The spectral changes are very similar to those observed for the natural graphite anodes cycled with $LiPF_6$ electrolyte and $LiNi_{1/3}Co_{1/3}Mn_{1/3}O_2$ cathodes.

The surface of the natural graphite anode after formation cycling with LiFOP electrolyte and a $LiFePO_4$ cathode contains higher concentrations of peaks characteristic of C—O and C═O than was observed with $LiPF_6$ electrolyte. This is consistent with the generation of a thicker anode SEI film with LiFOP electrolyte than with $LiPF_6$ electrolyte. After accelerated aging, the intensity of the peaks characteristic of C═O and C—O containing species are

Table 3
Elemental analysis of natural graphite anode cycled with $LiFePO_4$ cathode.

	C1s (%)	O1s (%)	F1s (%)	P2p (%)
Fresh NG	85.0	15.0		
Formed $LiPF_6$	54.3	24.6	19.6	1.5
Aged $LiPF_6$	41.3	30.8	23.3	4.6
Formed LiFOP	41.8	38.3	16.2	3.7
Aged LiFOP	25.5	42.6	26.9	5.0

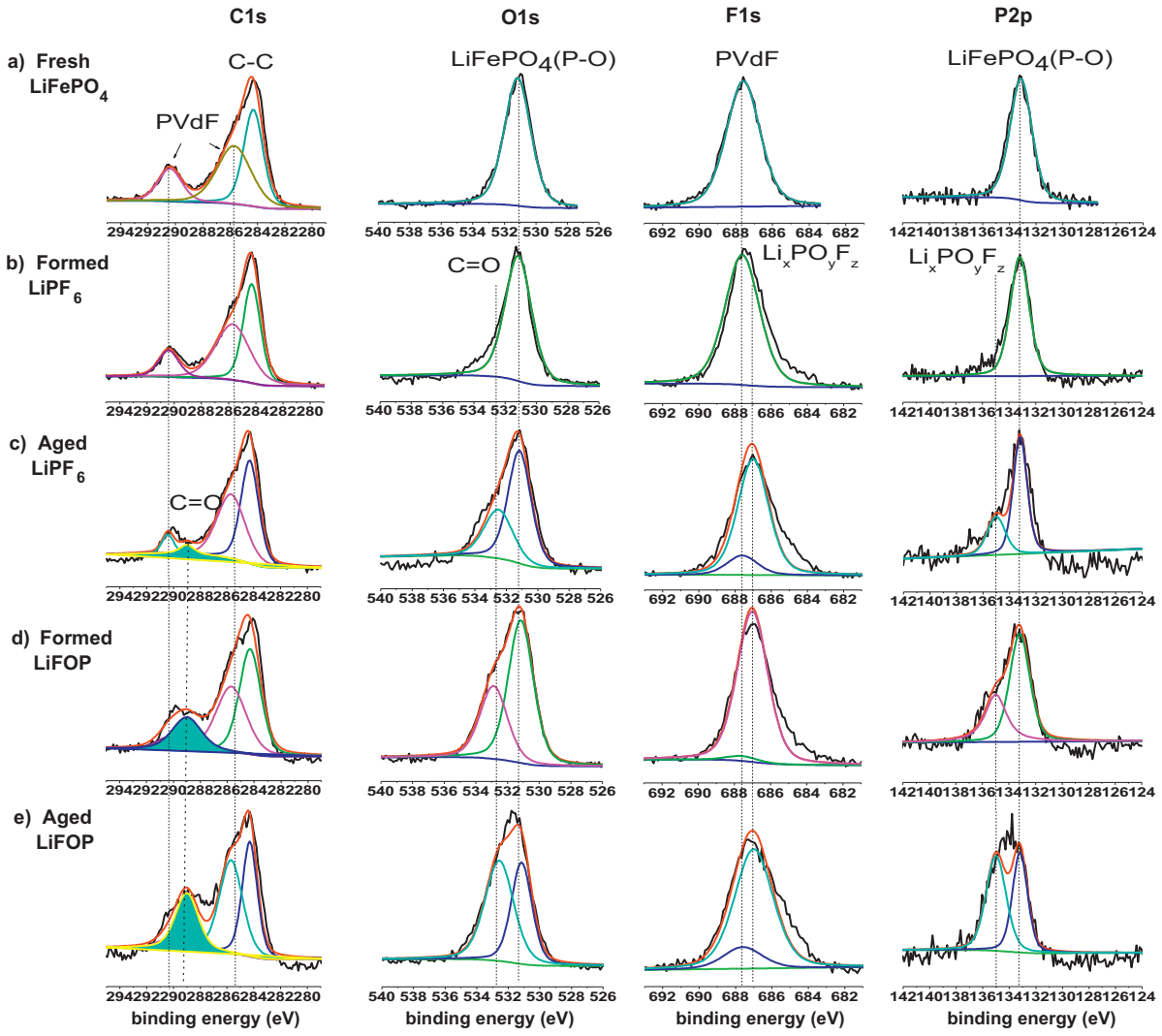

Fig. 10. XPS spectra of $LiFePO_4$ cathode (a) fresh; (b) formed with 1.2 M LiFOP in 3:7 EC/EMC; (c) formed with 1.2 M LiFOP in 3:7 PC/EMC; (d) aged with 1.2 M LiFOP in 3:7 EC/EMC; (e) aged with 1.2 M LiFOP in 3:7 PC/EMC.

further increased. The results are similar to that observed for natural graphite/$LiNi_{1/3}Co_{1/3}Mn_{1/3}O_2$ cells described above.

The XPS element spectra of $LiFePO_4$ cathodes fresh and cycled with natural graphite anodes are provided in Fig. 10 and the elemental concentrations are summarized in Table 4. The fresh $LiFePO_4$ cathode contains C1s peaks for graphite (284.3 eV) and PVDF (285.7 eV and 290.4 eV), an O1s peak for $LiFePO_4$ (531.2 eV), a F1s peak for PVDF (687.6 eV) and a P2p peak for $LiFePO_4$ (133.2 eV). Changes to the surface of the $LiFePO_4$ cathodes cycled with natural graphite and $LiPF_6$ or LiFOP electrolyte are similar to those observed with the natural graphite/$LiNi_{1/3}Co_{1/3}Mn_{1/3}O_2$ cells. The elemental concentrations of the cathodes extracted from cells after formation cycling or accelerated aging are similar to those of fresh $LiFePO_4$ cathode. After formation cycling or accelerated aging with LiFOP electrolyte the concentration of C is decreased and the concentration of O is increased on the $LiFePO_4$ surface. The changes in elemental concentration suggest that the surface film on the $LiFePO_4$ cathode is very thin in $LiPF_6$ electrolyte and thicker in the LiFOP electrolyte. The element spectra of the $LiFePO_4$ surfaces further support this assertion. The element spectra of the $LiFePO_4$ cathode cycled with $LiPF_6$ electrolyte and a natural graphite anode are very similar to the fresh $LiFePO_4$ cathode. The C1s spectrum of $LiFePO_4$ cathode after formation cycling and accelerated aging are similar and contain peaks characteristic of C—O and C═O containing species at 286.5 eV and 289.5 eV, respectively. The corresponding O1s peaks are also present at 533.5 eV and 531.5 eV. The changes to the $LiFePO_4$ cathode surface are similar to that observed on the surface of $LiNi_{1/3}Co_{1/3}Mn_{1/3}O_2$ cathodes as discussed above.

Table 4
Elemental analysis of $LiFePO_4$ cathode.

	C1s (%)	O1s (%)	F1s (%)	P2p (%)
Fresh $LiFePO_4$	57.9	18.4	17.7	5.5
Formed $LiPF_6$	53.7	21.7	19.7	4.9
Aged $LiPF_6$	52.5	23.0	19.4	5.1
Formed LiFOP	48.8	29.7	15.3	6.2
Aged LiFOP	41.0	32.9	20.4	5.6

3.4. FT-IR spectra

FT-IR spectra of natural graphite anode fresh and cycled with $LiNi_{1/3}Co_{1/3}Mn_{1/3}O_2$ cathode are depicted in Fig. 11. The absorption bands in the spectrum of fresh natural graphite result from the CMC and SBR binders. The IR spectrum of the anode after formation cycling with $LiPF_6$ electrolyte appears very similar to the fresh natural graphite anode. The IR spectrum of the natural graphite

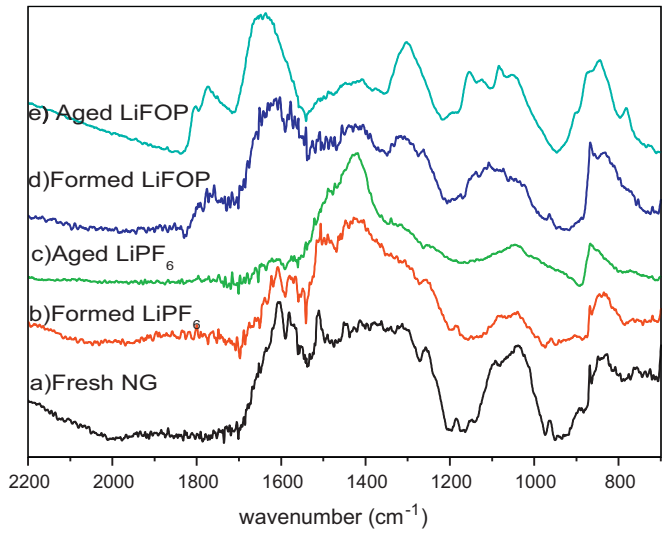

Fig. 11. FT-IR spectra of natural graphite anode cycled with $LiNi_{1/3}Co_{1/3}Mn_{1/3}O_2$ cathode (a) fresh; (b) formed with 1.2 M $LiPF_6$ in 3:7 EC/EMC; (c) formed with 1.2 M LiFOP in 3:7 PC/EMC; (d) aged with 1.2 M $LiPF_6$ in 3:7 EC/EMC; (e) 1.2 M LiFOP in 3:7 PC/EMC.

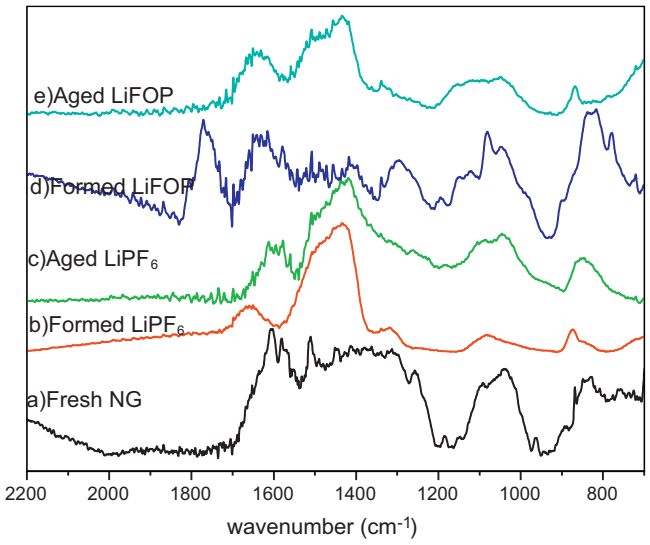

Fig. 13. FT-IR spectra of natural graphite anode cycled with $LiFePO_4$ cathode (a) fresh; (b) formed with 1.2 M $LiPF_6$ in 3:7 EC/EMC; (c) formed with 1.2 M LiFOP in 3:7 PC/EMC; (d) aged with 1.2 M $LiPF_6$ in 3:7 EC/EMC; (e) 1.2 M LiFOP in 3:7 PC/EMC.

anode after accelerated aging with the $LiPF_6$ electrolyte contains an additional peak at 1427 cm^{-1} characteristic of lithium carbonate.

The IR spectrum of the natural graphite anode after formation cycling with LiFOP electrolyte is quite different from that of the natural graphite anode after formation cycling with $LiPF_6$ electrolyte. The presence of lithium oxalate is supported by a peak at ~1640 cm^{-1} and poly(ethylenecarbonate) is supported by a peak at 1760 cm^{-1}. After accelerated aging the intensity of the peaks for lithium oxalate and poly(ethylenecarbonate) increase and a new absorption at ~1300 cm^{-1} characteristic of lithium alkyl carbonates is observed.

Fig. 12 contains the FT-IR spectra of $LiNi_{1/3}Co_{1/3}Mn_{1/3}O_2$ cathode fresh and after cycling with a natural graphite anode. The peaks of PVdF binder are observed at 1400 cm^{-1}, 1175 cm^{-1} and 879 cm^{-1} on the fresh $LiNi_{1/3}Co_{1/3}Mn_{1/3}O_2$ cathode. The IR spectra of the cathode after formation cycling or accelerated aging with $LiPF_6$ electrolyte are very similar to the IR spectra of the fresh $LiNi_{1/3}Co_{1/3}Mn_{1/3}O_2$ cathode. The IR spectra of the $LiNi_{1/3}Co_{1/3}Mn_{1/3}O_2$ cathode after formation cycling or accelerated aging with LiFOP electrolyte contain an additional absorption at 1640 cm^{-1} characteristic of lithium oxalate. The results are consistent with the XPS data of $LiNi_{1/3}Co_{1/3}Mn_{1/3}O_2$ cathodes cycled with LiFOP electrolyte.

FT-IR spectra of natural graphite anode fresh and cycled with $LiFePO_4$ cathode are provided in Fig. 13. The IR spectra of the natural graphite after formation cycling with $LiPF_6$ electrolyte contain new absorptions at 1440 cm^{-1} and 1650 cm^{-1} characteristic of lithium carbonates and lithium alkyl carbonates, respectively. The IR spectrum after accelerated aging with $LiPF_6$ electrolyte is similar to the spectrum after formation cycling.

The IR spectra of a natural graphite anode after formation cycling with LiFOP electrolyte contains a similar peak at 1650 cm^{-1} consistent with the presence of lithium alkylcarbonates or lithium oxalate and an additional peak at 1780 cm^{-1} characteristic of

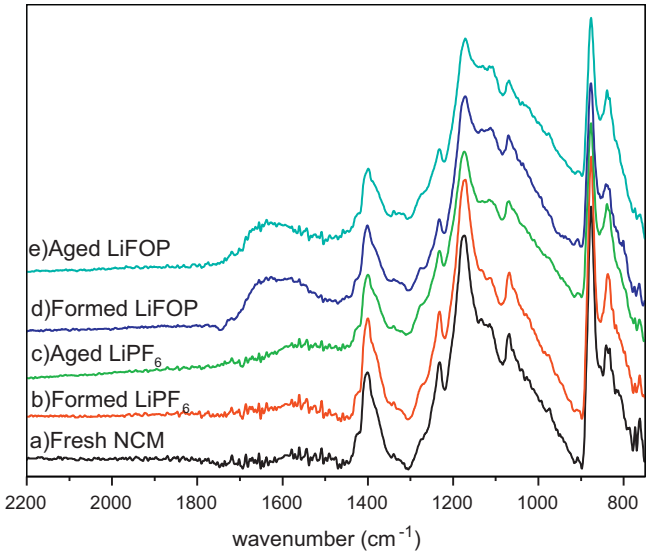

Fig. 12. FT-IR spectra of $LiNi_{1/3}Co_{1/3}Mn_{1/3}O_2$ cathode (a) fresh; (b) formed with 1.2 M $LiPF_6$ in 3:7 EC/EMC; (c) formed with 1.2 M LiFOP in 3:7 PC/EMC; (d) aged with 1.2 M $LiPF_6$ in 3:7 EC/EMC; (e) 1.2 M LiFOP in 3:7 PC/EMC.

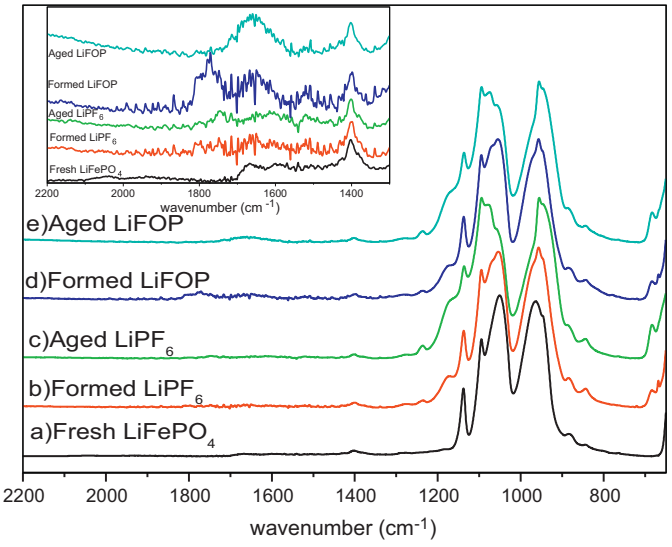

Fig. 14. FT-IR spectra of $LiFePO_4$ cathode (a) fresh;(b) formed with 1.2 M $LiPF_6$ in 3:7 EC/EMC; (c) formed with 1.2 M LiFOP in 3:7 PC/EMC; (d) aged with 1.2 M $LiPF_6$ in 3:7 EC/EMC; (e) 1.2 M LiFOP in 3:7 PC/EMC.

poly(ethylenecarbonate). After accelerated aging the peak of poly(ethylenecarbonate) is no longer observed and a new peak is observed at 1442 cm^{-1} suggesting the presence of Li_2CO_3. The changes in the composition of the anode SEI is consistent with significant damage occurring to the SEI during the aging process.

A similar trend is observed in the IR spectra of the $LiFePO_4$ cathodes as depicted in Fig. 14. The spectral region from 800 to 1200 cm^{-1} is dominated by the P—O absorptions of $LiFePO_4$. An inset highlighting the IR spectral region between 2200 cm^{-1} and 1300 cm^{-1} is included in Fig. 14. The IR spectra of the $LiFePO_4$ cycled with $LiPF_6$ electrolyte are very similar to the fresh cathode suggesting very little change to the surface. The IR spectrum of the $LiFePO_4$ cathode after formation cycling with LiFOP electrolyte contains additional peaks at 1650 and 1780 cm^{-1} suggesting that lithium oxalate and poly(ethylenecarbonate) are present. After accelerated aging of the $LiFePO_4$ cathode with the LiFOP electrolyte, the peak for poly(ethylenecarbonate) is no longer observed while the lithium oxalate is retained.

4. Conclusions

The use of propylene carbonate (PC) in lithium battery electrolytes has been limited due to graphite exfoliation in the presence of $LiPF_6$/PC electrolytes. The use of the novel lithium salt lithium tetrafluorooxalatophosphate (LiFOP) allows reversible cycling with PC based electrolytes. The low temperature cycling performance of cells with LiFOP/PC electrolyte is superior to similar $LiPF_6$/EC electrolytes. However, after accelerated aging the room temperature performance of cells with LiFOP/PC electrolyte is inferior to $LiPF_6$/EC electrolytes after accelerated aging. Surface analysis of cells after formation cycling suggests that LiFOP/PC electrolytes generate a unique and stable anode SEI which prevents graphite exfoliation by PC due to the presence of lithium oxalate. Surface analysis of samples after accelerated aging indicate that the SEI film formed on the cells cycled with LiFOP/PC electrolyte is significantly damaged during accelerated aging leading to decreased capacity retention.

Acknowledgement

We would like to thank the BATT program sponsored by the DOE Vehicle Technologies Program for financial support of this research.

References

[1] M. Armand, J.-M. Tarascon, Nature 451 (2008) 652.
[2] K. Xu, Chem. Rev. 104 (2004) 4303.
[3] M.C. Smart, B.V. Ratnakumar, K.B. Chin, L.D. Whitcanack, J. Electrochem. Soc. 157 (2010) A1361.
[4] K. Xu, J. Electrochem. Soc. 156 (2009) A751.
[5] A. Xiao, L. Yang, B.L. Lucht, Electrochem. Solid-State Lett. 10 (2007) A241.
[6] M. Xu, A. Xiao, W. Li, B.L. Lucht, Electrochem. Solid-State Lett. 12 (2009) A155.
[7] M. Xu, A. Xiao, W. Li, B.L. Lucht, J. Electrochem. Soc. 157 (2010) A115.
[8] L. Zhou, S. Dalavi, M. Xu, B.L. Lucht, J. Power Sources 196 (2011) 8073.
[9] M. Xu, L. Zhou, D. Chalasani, S. Dalavi, B.L. Lucht, J. Electrochem. Soc. 158 (2011) A1202.
[10] K. Xu, U. Lee, S.S. Zhang, T.R. Jow, J. Electrochem. Soc. 151 (2004) A2106.
[11] S. Zugmann, D. Moosbauer, M. Amereller, C. Schreiner, F. Wudy, R. Schmitz, R. Schmitz, P. Isken, C. Dippel, R. Müller, M. Kunze, A. Lex-Balducci, M. Winter, H.J. Gores, J. Power Sources 196 (2011) 1417.
[12] S.S. Zhang, Electrochem. Commun. 8 (2006) 1423.